In-situ magnetic resonance imaging highlights local bovine meat structural changes during heating

Mustapha Bouhrara, Sylvie Clerjon, Jean-Louis Damez, J.-M. Bonny

IN-SITU MAGNETIC RESONANCE IMAGING HIGHLIGHTS LOCAL BOVINE MEAT STRUCTURAL CHANGES DURING HEATING

M. Bouhrara, S. Clerjon, J.L. Damez and J.M. Bonny

INRA, UR370 Qualité des Produits Animaux, F-63122 Saint Genès Champanelle, France.

Abstract – Understanding and monitoring deformation and water content changes in meat during cooking is of prime importance for product quality. We show here some possibilities offered by Nuclear Magnetic Resonance Imaging (MRI) for *in situ* dynamic measurement of deformation fields and water content mapping during beef heating from 20 to 75 °C. MR Images were acquired during heating and images registration was used to calculate the deformation field. The temperature distribution in the sample was simulated numerically to link structural modifications and water transfer with temperature timecourses. During heating, proton density decreases because of magnetic susceptibility drop with temperature rise and water expulsion due to muscle contraction. A positive relation was also found between local cumulative deformation and water content. This new approach makes it possible to map the deformation fields and water content dynamically and simultaneously, and trace thermal history to build heuristic models linking these parameters.

Key Words – Dynamic and quantitative MRI, deformation, cooking loss, structure, water content.

I. INTRODUCTION

Control of the sensory, nutritional and technological qualities of cooked meat products is of prime importance for both consumers and industry. Juiciness has been reported to be correlated with tenderness, the main palatability trait, water loss leading to higher perceived toughness, as the juices act as a sort of lubricant during mastication (1).

In addition to the simple measurement of cooking loss, Magnetic Resonance Imaging (MRI) makes it possible to dynamically map water content during the heating process. It opens new paths for observing detailed changes in muscle structure and water transfer simultaneously. To achieve this, we introduced a novel MRI-compatible device, which heats the sample via a fluid, and a strategy based on the dynamic acquisition of images showing the contrast between muscle fibers and intramuscular connective tissue (2). Tracking these fiducial markers allowed reconstructing of the required deformation maps (3). We also mapped water content (i.e. proton spin density, PD) by MRI and temperature by numerical simulation. The quantitative relationships between deformation, water and temperature were inferred in different regions of the sample and were then averaged in global models.

These models give new information about the underlying mechanisms of meat deformation during heating and to associated water transfers.

II. MATERIALS AND METHODS

Two samples were cut in *Biceps femoris* (BF) coming from Charolais cows, in the form of cylinders 5 cm in diameter by 6 cm in length, with the muscle fibers oriented axially. We chose this muscle because of its richness in elastin which is visible by T_2*-weighted MRI. The meat cylinders were then placed in plastic bags in a vacuum to prevent direct contact with the circulating heating water. For each sample, our analyses were performed on five transverse slices which intercepted the muscle fiber axis perpendicularly.

Each sample was heated over the temperature range 20–75 °C, with a constant gradient of 0.63 °C/min, using water circulating in an MRI-compatible device. This low temperature gradient was chosen for being compatible with our MRI acquisition times.

Image acquisition was carried out using a Biospec horizontal 4.7 T MRI system (Bruker, Germany), with a 26 cm diameter bore, equipped with a BGA-26 rapid gradient system and using a linear polarized birdcage coil for both emission and reception. To construct deformation maps, a set of images was acquired for highlighting contrast between muscle fibers and intramuscular connective tissue. To do this, T_2*-weighted images sensitive to differences of the magnetic

susceptibility produced by the fiber-connective tissue interfaces inside the muscle were required. The protocol is carefully described in (3).

The next step was to reconstruct the deformation fields of the sample from two successively acquired T_2*-weighted images. The deformation field at temperature t_i is the mapped vector field resulting of the local transformations applied to pass from the image obtained at temperature $t_{(i-1)}$ to that obtained at temperature t_i. We demonstrated previously that a 2D fourth order polynomial spatial transformation is adequate for modeling muscle deformation during heating (3). Following this, the degrees-of-freedom of this transformation were estimated by minimizing the difference between two successive T_2*-weighted images using an Automated Image Registration package. This registration is possible because the internal fiducial markers appeared in the T_2*-weighted images throughout the heating process. Finally, the deformation field $\mathbf{w}(t_i)$ was inferred by computing the two components of 2D displacement in each voxel position of the image.

The second set of images was dedicated to PD mapping. The protocol was based on the use of fast imaging method (spin-echo echo-planar technique) for obtaining T2 relaxation time and water content of tissues (4).

At high magnetic field, the interactions between the active emission RF field B_1 and the (muscle) sample caused inhomogeneity of B_1 which was no longer negligible, biasing the determination of PD. Since B_1 distribution depends on several unknown and evolving factors, B_1 was mapped during heating (4, 5).

Temperature maps were obtained from numerical simulations and validated by comparison with invasive measurements (2).

Finally we constructed average models from local information provided by deformation, proton density and temperature maps. Each voxel in the image obtained at 20 °C was tracked by successively applying the transformation $\mathbf{w}(t_i)$. Deformation, PD and temperature were collected from each quantitative map along this trajectory as a function of time t_i. Such local relations were then averaged for all voxels to obtain more general laws.

It is also interesting to know the impact of temperature on the final deformation, which corresponds to the accumulation of deformations occurring between two successive images. All our samples were heated from 20 to 75 °C. Despite this, at the end of cooking, few voxels had effectively reached 75 °C. Thus to ensure robustness, the average models were only defined up to 70 °C.

To quantify the correlation between the PD and the cumulative deformation, several regions of interest (ROIs) were defined manually for each of the 5 slices of each sample and for the last two images of our acquisition series, presenting the highest average temperatures (~70 °C) and thus the highest cumulative deformation and PD. A homogenous deformation zone was chosen for the ROIs and the average cumulative deformation and the corresponding PD in each ROI were calculated. All the numerical procedures were performed with Matlab (MathWorks Inc., Natick, USA).

III. RESULTS AND DISCUSSION

Figure 1 shows T2*-weighted images, temperature maps, deformation fields and PD maps obtained at 5 average temperatures and in the central slice (3/5) of the sample. It validates two important hypotheses: (i) T2*-weighted images clearly show internal fiducial markers at each temperature despite the difficult experimental conditions which lead to to the continuous loss of SNR (Fig. 1-A), (ii) temperature is inhomogenously distributed (Fig. 1-B) and leads to significant spatial variation of both deformation and PD. Under these conditions, the spatial registration step converged regardless of the temperature and resulted in a robust estimation of the deformation fields in direction and magnitude (Fig. 1-C). For a better readability, the gray levels were adjusted on figures 1-A, -D to compensate for continuous SNR loss.

Cumulative deformation versus temperature is given on Figure 2. Before 40 °C, cumulative deformation is very slight (0.01 mm/°C) and corresponds to the accumulation of the image registration error during field deformation computation (3). From this, a shallow slope can be observed before an inflexion point (see AD on Fig. 2) marking an acceleration of the deformation. Local information reveals a moderate strain between ~ 38 °C and ~ 58 °C.

This phase corresponds to myosin denaturing and the beginning of collagen denaturing (6),

explaining the slight deformation observed. During this phase, juice is essentially transferred

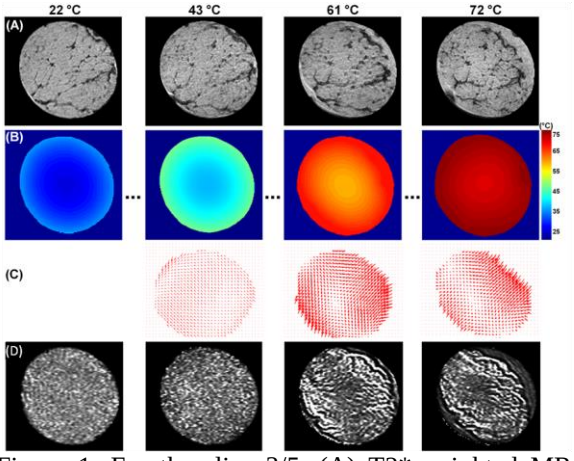

Figure 1. For the slice 3/5: (A) T2*-weighted MR images. Corresponding (B) temperature maps (numerical simulation), (C) deformation as a function of direction and magnitude, (D) Proton Density maps.

to interfascicular spaces within the muscle (2, 7). The acceleration of deformation is due to the heating of sarcoplasmic proteins, leading to their denaturing, as reported by Hoult (8), and therefore to a reduction of the mechanical resistance of the myofibers to mechanical stress. At the same time, the contraction of collagen leads to mechanical constraints that in turn lead to the contraction of the connective network. Water is then expelled outside the sample, visible as a surrounding hypersignal in Figure 1-A, which explains the strong deformation observed. Plateaus of deformations that occur from ~ 68 °C can be explained by the end of one or several of these phenomena.

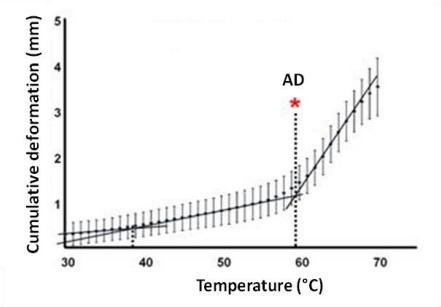

Figure 2. Cumulative deformation (mm) versus temperature (°C). Error bars represent the standard deviation. The AD marks the inflexion point.

As shown in Figure 3, the PD in the muscle considerably decreases with temperature. We observed a linear loss of 2%/°C up to 65-67 °C, which tended to be greater close to 70 °C. These losses led to a reduction of total PD during cooking from 60 to 83% depending on the sample. This reduction is in part due to Curie's law that states that the measured magnetization is inversely proportional to temperature (9). The reduction of PD with temperature can also be explained by contraction that expels intramuscular water outside the muscle. The quantification of final water loss (2) permits explaining approximately 40% of the reduction of PD. It should be noted that the large standard deviations reflect the noise propagated on the maps of PD (Fig. 1-D). In spite of this, the high number of voxels per slice (more than 10000) endows statistic robustness to the presented averaged values.

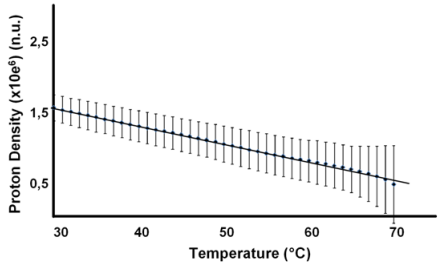

Figure 3. Proton density versus temperature (°C). Error bars represent the standard deviation.

An original aspect of our approach is that it provides a direct and average relation between deformation and water content.

Figures 1 seems to show a correlation between the deformation modulus (line C) and PD (line D) at high temperatures. A preliminary study has shown that there is no correlation between deformation and PD when comparing measurements voxel by voxel due to considerable spatial variations of PD (contrary to deformation). Part of this variability is due to the presence of mobile water in the interfascicular spaces, which remains visible in spite of the effect of partial volume (2). We therefore chose to average PD in ROIs to reduce this variability. This approach highlights the Spearman's correlation coefficient R^2 of the order 0.63 to 0.70 depending on the sample. Figure 4 shows that the most deformed zones are those where PD is highest which may seem counterintuitive, though consistent with the poroelastic theory. This theory applies to meat

during cooking, but in this case it is supplemented with a constitutive equation for the pressure exerted by the contracting protein network during heating on the interstitial fluid (10). In this study, the interpretation was based on the Darcy's law which describes how water migrates from a high pressure area to a low pressure area. In the case of meat cooking, because of muscle contractions, the pressure in the muscle becomes higher than the external pressure, thus causing water to transfer from the sample towards the exterior. Moreover, at the superficial area of the sample, the temperature is higher than at the center, leading to the creation of interfascicular channels that may "trap" the migrating water. It is worthwhile noting that our method is dynamical and thus gives several images of PD along the heating process. This feature has no equivalent, since water content in cooked meat is classically studied at the end of the heating process.

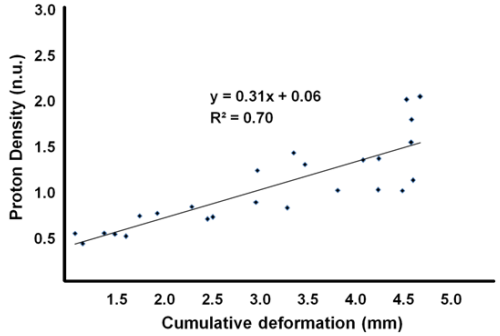

Figure 4. Cumulative deformation (mm) versus temperature (°C).

IV. CONCLUSION

The work presented here is pioneering since it focuses on the simultaneous mapping of deformation, water content and temperature during cooking. However, both inter-animal variation and muscle type are likely to have important effects which deserve further studies on different muscle types, coming from different animals.

Within the framework of developing industrial cooking, it would be possible to study the effect of mechanical prestressing, mainly which is exerted during maturation, on deformation during cooking, which is another issue of interest to industry. The role of ingredients is also fundamental, for example the effects of salting on cooking are of interest for the pork processing industry. Lastly, *in situ* monitoring of structural changes during cooking should be applied to all foods for which cooking is the decisive parameter for final quality.

ACKNOWLEDGEMENTS

The MRI experiments were performed at the biological systems MR platform at the INRA center of Clermont-Ferrand, France (www.clermont.inra.fr/rmsb/). This work was founded by the CE project ProSafeBeef.

REFERENCES

1. Tornberg, E. Effects of heat on meat proteins—Implications on structure and quality of meat products. Meat Science 2005, 70, 493-508.
2. Bouhrara, M., Clerjon, C., Damez, J.L., Chevarin, C., Portanguen, S., Kondjoyan., & Bonny, J.M. Dynamic MRI and thermal simulation to interpret deformation and water transfer in meat during heating. Journal of Agricultural and Food Chemistry 2011, 59, 1229-1235.
3. Bouhrara, M., Lehallier, B., Clerjon, C., Damez, J.L., & Bonny, J.M. Mapping of muscle deformation during heating: in situ dynamic MRI and nonlinear registration. Magnetic Resonance Imaging 2012, 30, 422-430.
4. Bouhrara M., Clerjon S., Damez JL, & Bonny JM. (2012). In-situ imaging highlights local structural changes during heating: the case of meat. Journal of Agricultural and Food Chemistry, in press.
5. Bouhrara, M., & Bonny, J.M. B1 mapping with selective pulses. Magnetic Resonance in Medicine 2012, DOI 10.1002/mrm.24146.
6. Martens, H., Stabursvik, E., & Martens, M. Texture and colour changes in meat during cooking related to thermal denaturation of muscle proteins. Journal of Texture Studies 1982, 13, 291-309.
7. Straadt, I. K., Rasmussen, M., Andersen, H. J., & Bertram, H. C. Aging-induced changes in microstructure and water distribution in fresh and cooked pork in relation to water-holding capacity and cooking loss - A combined confocal laser scanning microscopy (CLSM) and low-field nuclear magnetic resonance relaxation study. Meat Science 2007, 75, 687-695.
8. Hoult, D. I., & Lauterbur, P. C. The Sensitivity of the Zeugmatographic Experiment Involving Human Samples. Journal of Magnetic Resonance 1979, 34, 425-433.
9. Abragam, A. The principles of the nuclear magnetism; New York: Oxford University Press 1983, pp 599.
10. Van der Sman, R. G. M. Moisture transport during cooking of meat: An analysis based on Flory-Rehner theory. Meat Science 2007, 76, 730-738.